CoreID JOURNAL

Vol. 2 No. 2, July 2024 (45-51)
ISSN: 2987-6990
DOI: https://doi.org/10.60005/coreid.v2i2.32

Hyperbolic Lattice Boltzmann Method and Quantum Modelling of Nanostructures: A Numerical Framework for Femtosecond Laser Induced Periodic Surface Structures

Derren Audric Sudarto[1], Ikhsan Mochammad Noor[2]
[1,2] Faculty of Mechanical and Aerospace Engineering, Bandung Institute of Technology, Indonesia

Article Info

Article history:
Received May 30, 2024
Revised July 15, 2024
Accepted July 26, 2024

Keywords:
Lattice Boltzmann,
Ultrashort Laser,
Quantum Mechanics,
Two-Temperature Model,
Laser Induced Periodic Surface Structures (LIPPS)

ABSTRACT (10 PT)

This paper presents a numerical analysis of laser induced periodic surface structures (LIPSS) using lattice Boltzmann method. The Cattaneo-Vernotte hyperbolic heat conduction model is used to derive the hyperbolic lattice Boltzmann in order to consider the non-Fourier effect in conduction. A Gaussian ultrashort laser is induced on a thin film with varying length in the nanoscale. The energy transfer within the material is governed by the two temperature model which calculates the evolution of electron and lattice temperatures. The thermal and optical properties of the nanostructure is modelled based on quantum mechanics theory. The resultant nondimensional temperature and ablation profile are compared to experimental and other numerical methods data. Additionally, the effect of parallel computing is shown..

Corresponding Author:

Ikhsan Mochammad Noor
Faculty of Mechanical and Aerospace Engineering, Bandung Institute of Technology, Indonesia
Jl. Ganesa No.10, Lb. Siliwangi, Kecamatan Coblong, Kota Bandung, Jawa Barat 40132
Email: 20923305@mahasiswa.itb.ac.id

1. INTRODUCTION

Ultrashort laser pulses produce ultra-high peak fluences with ultra-short pulse width duration that are in order of picosecond (10^{-12}s) to femtosecond (10^{-12}s) which enable precise and efficient fabrication on material surfaces. This technology has found its uses in procuring unique and advanced properties in multidisciplinary research such as optics modification, plasmonics [1], wettability, hydrodynamics drag reduction, tissue ablation [2], laser surgery [3], and nanodevices manufacturing [4] that are otherwise improbable with short lasers in the nanosecond regime.

The interaction between ultrashort pulses and material matters such as metals, semiconductors, and dielectrics [5], produces a phenomenon known as laser induced periodic surface structures (LIPSS) [6]. When fluences are above the ablation threshold, the resultant topography near the material surface is a complex phenomenon [7] attributable to numerous ablation mechanisms, such as nanospallation, phase explosion, vaporization, fragmentation, and capillary effects.

The intriguing capability of ultrashort lasers underlies complex physics concepts, encovering topics such as nonlinear optics, electromagnetics, and quantum mechanics. The interaction with a matter occurring in an ultra-short timescale ensues unconventional energy transfer, nonlinear optical and thermal properties, and laser ablation. When ultrashort pulses are induced, the thermalization of electrons occurs rather quickly, before the absorbed energy is transferred again towards the lattices [8]. This phenomenon takes place due to the relative duration of the electron-lattice relaxation time and the pulse width being similar, thus the evolution of both electron and lattice properties having separate calculations becomes justified. Jiang [9] argued that when the electrons temperature becomes similar to the fermi temperature of a material, the interaction between electron distribution deviates from the free electron model which leads to modifications of optical properties.

Modeling of thermal and optical properties with quantum mechanics [10] then becomes imperative for higher laser fluences where ablation occurs.

2. METHOD

2.1 Governing Equations

2.1.1 Two Temperature Model

The temperatures of electron T_e and lattice T_l are governed by the Two Temperature Model (TTM) [11]. The energy conservation law can be written as

$$C_e \frac{\partial T_e}{\partial t} = -\frac{\partial q_e}{\partial x} - G(T_e - T_l) + S(x,t) \quad (1)$$

$$\tau_e \frac{\partial q_e}{\partial t} + q_e = -k_e \frac{\partial T_e}{\partial x} \quad (2)$$

$$C_l \frac{\partial T_l}{\partial t} = -\frac{\partial q_l}{\partial x} + G(T_e - T_l) \quad (3)$$

$$\tau_l \frac{\partial q_l}{\partial t} + q_l = -k_l \frac{\partial T_l}{\partial x} \quad (4)$$

Where C is the specific heat capacity, q is energy flux, τ is relaxation time, k is thermal conductivity, G is electron-lattice coupling factor, and S is energy absorbed from the laser.

a) Quantum Modelling

The nonequilibrium thermal properties C_e, C_l, k_e, and k_l are function of their temperatures. Considering electron temperatures similar to Fermi temperature T_f, the average number of electrons with energy state ε_e is following the Fermi-Dirac distribution.

$$\langle n_k \rangle = \frac{1}{\exp(\beta[\varepsilon_k - \mu]) + 1} \quad (5)$$

where $\beta(T_e) = 1/k_b T_e(t,x)$ and μ is chemical potential. The distribution given in equation 5 is a good approximation at high temperatures and when the pulse duration is higher than the relaxation time of the electron. This is because when a femtosecond laser pulse has pulse duration smaller than the electron relaxation time, the Fermi-Dirac distribution can be disrupted. By calculating the average kinetic energy per electron ⟨n⟩ [9] from equation 5, the heat capacity of electron can be obtained.

$$C_e = n_e \left(\frac{\partial \langle \varepsilon \rangle}{\partial T_e}\right)_V \quad (6)$$

The thermal conductivity of electron can be determined from the Drude theory of metals:

$$k_e(T_e) = \frac{1}{3} v_e^2(T_e) \tau_e(T_e) C_e(T_e) \quad (7)$$

where v_e is the average electron speed. Note that v_e and C_e are obtained from the Fermi-Dirac distribution. Meanwhile, the electron relaxation time τ_e can be determined by considering the metal as dense plasma during high fluence ablation. The electron conductivity model can be derived from the Boltzmann transport equation [12]

$$\begin{aligned} \tau_e(x,y,t) \quad &= \frac{3}{2\sqrt{2}\pi} \frac{(k_b T_e(x,y,t))^{3/2}}{(Z^*)^2 n_e e^4 \ln\Lambda} \\ &\times [1 + \exp - \mu/k_b T_e(x,y,t)] F_{1/2} \end{aligned} \quad (8)$$

where e is electron charge and Z^* is ionization state and is a material constant. $F_{1/2}$ is the Fermi Integral and $ln\Lambda$ is the Coulomb logarithm.

The lattice heat capacity can be determined by the Debye model [9]. The average kinetic energy of the lattice can be determined by

$$\langle \varepsilon_k \rangle = \int_0^{\upsilon_{max}} \frac{6\pi h}{n_a c_s^3} \frac{\upsilon^3}{\exp h\upsilon/k_b T_l - 1} d\upsilon \quad (9)$$

where n_a is the phonon number density and υ_max is maximum frequency of phonon.
The heat capacity of the lattice (phonon) can then be calculated by

$$C_l(T_l) = 2n_a \left(\frac{\partial \langle \varepsilon_k \rangle}{\partial T_l}\right)_V \tag{10}$$

b) Electron-Phonon Coupling

The rate of energy transfer from electron to lattice is quantified by $G(T_e\text{-}T_l)$ is a function of temperature. The value of G can be obtained by

$$G = G_{RT}\left[\frac{A_e}{B_l}(T_e + T_l) + 1\right] \tag{11}$$

Where G_{RT} is a constant obtained by assuming Fermi-Dirac distribution for electrons and Bose-Einstein distribution for lattices [13], while A_e and B_l are material constants.

c) Laser Source

The laser source is modeled after the spatiotemporal Gaussian distribution, which is the most commonly used for ultrashort laser research due to its realistic representation and mathematical convenience. This representation is given by

$$\begin{aligned} S(x,y,t) \quad &= 0.94J \frac{1-R}{t_p(\delta+\delta_b)[1-e^{(-L/(\delta+\delta_b))}]} \\ &\times \exp\left[\frac{L-x}{\delta+\delta_b} - 2.77\left(\frac{t}{t_p}\right)^2\right] \\ &\times \exp(-2y^2/w_0^2) \end{aligned} \tag{12}$$

In a two dimensional domain, x and y is the position in terms of thickness and length of the structure, respectively. The maximum laser fluence is J. The material optical properties are the reflectivity R, penetration depth δ, and ballistic range δ_b. L denotes the characteristic length (thickness) of the structure. The pulse waist size is given by w_0, and the duration of the pulse is represented by the Full-Width at Half-Maximum (FWHM) duration t_p.

The last term in equation 12 represents the spatial profile [14] which can be modified for one and three dimensional cases.

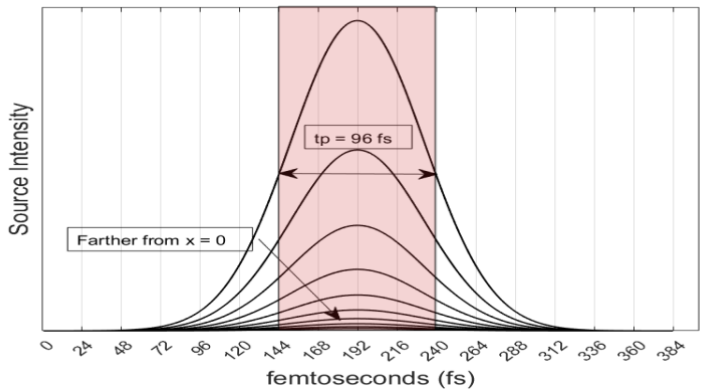

Figure 1: Temporal profile of Gaussian Laser with t_p=96fs. The intensity is maximum at t=2t_p. Due to optical properties of the material, the intensity reduces as the laser source is farther away from the surface

2.1.2 Hyperbolic Heat Equation

In order to capture the nonlinear heat conduction effect, a hyperbolic Lattice Boltzmann is derived based on the Cattaneo-Vernotte model. The CV model is a non-Fourier heat conduction equation, derived by Cattaneo

and Vernotte independently in the mid 20th century based on the kinetic gas theory [15], [16]. The CV equation was proposed in light of the nonphysical behavior of the conventional Fourier's Law of Conduction when observed at very low temperatures. It was discovered in other cases such as ultrafast heating and heating in heterogeneous materials that the assumption of infinite propagation heat velocity from Fourier's law becomes invalid, thus resulting in inaccurate results [17]. The relaxation time τ_q is introduced to the existing Fourier's model to represent the finite propagation speed. Inserting the CV model in the energy equation yields the following.

$$\tau_q \frac{\partial^2 T}{\partial t^2} + C \frac{\partial T}{\partial t} = \frac{\partial}{\partial x}\left(k \frac{\partial T}{\partial x}\right) + S + \tau_q \frac{\partial S}{\partial t} \tag{13}$$

2.2 Numerical Model

2.2.1 Lattice Boltzmann Method

From the CV equation, the hyperbolic lattice Boltzmann method is derived by considering the temperature evolution [18]. The external source is also modified such that the term *G(T)* is also considered. The new LB equation becomes

$$\begin{aligned} \Psi_i - \phi\Psi_i^0 &= -2(\varphi+\phi)\Theta_i + 2\phi\Theta_i^0 \\ &\quad + \frac{G\Delta t}{C}(f_i - \phi f_i^0) + \frac{w_i \Delta t}{C}(S_i - \phi S_i^0) \end{aligned} \tag{14}$$

where the distribution functions are denoted by

$$\begin{aligned} \Psi_i(x,t) &= f_i(x+\Delta x, t+\Delta t) - f_i(x,t) \\ \Theta_i(x,t) &= f_i(x,t) - f_i^{eq}(x,t) \\ \Psi_i^0 &= \Psi_i(x, t-\Delta t) \\ \Theta_i^0 &= \Theta_i(x, t-\Delta t) \end{aligned} \tag{15}$$

Moreover, ϕ and φ are relaxation times given by

$$\phi = \frac{\Gamma}{2\alpha+1+\Gamma} \varphi = \frac{1}{2\alpha+1+\Gamma} \tag{16}$$

where α is thermal diffusivity and $\Gamma=\tau/\Delta t$. The LB method given in equation 14 reduces to parabolic which follows Fourier's Law when $\Gamma \rightarrow 0$.

2.2.2 Initial Condition and Boundary Treatment

The initial condition for the material is set at room temperature $T_{e0}=T_{l0}=300K$. Since the timescale is within the pico- to femto-second, heat loss on the boundaries are negligible [19]. The boundaries on the domain are assumed to be adiabatic and can be described by

$$\left(\frac{\partial T_e}{\partial n}\right)_\Omega = \left(\frac{\partial T_l}{\partial n}\right)_\Omega = 0 \tag{17}$$

2.2.3 Computational Domain

For this research, a $N_x \times N_y = 100 \times 100$ grid is used for computational domain. The diameter of the Gaussian laser is set to be $N_x/2$, with its spot located on the centre. The material chosen is gold, and calculation for its thermal and reflective properties can be obtained from literature. The laser fluence is set to be $J=10J/m^2$, with pulse width of $t_p=96fs$ (shown in Fig. 1). The thickness of the gold film is $d=100nm$.

3. RESULT AND DISCUSSION

The simulation results are compared to experiment data [20]. The first data in Fig. 2 compares the non-dimensional electron temperature θ_e on the surface which can be calculated by $\theta_e=(T_e-T_e0)/(T_e-T_e0)_{max}$.

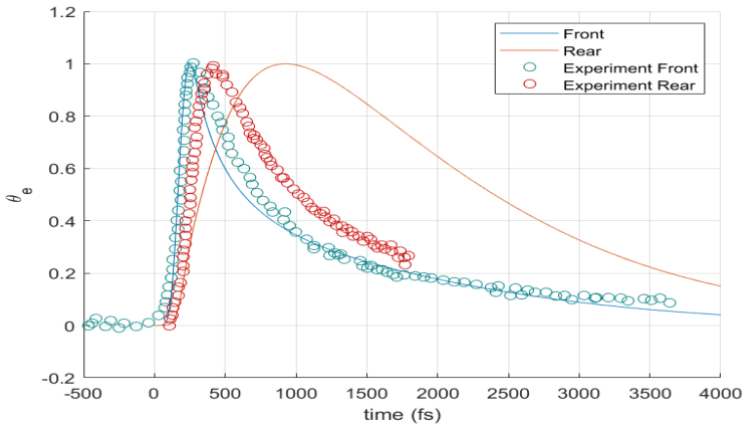

Figure 2: Normalized electron temperature in the front surface and rear surface of gold for $K = 10J/m^2$, $d = 100nm$. Experiment data by Brorson and group, 1987 [20]

It can be observed that for the current progress, the numerical code captures the electron temperature evolution accurately on the front surface. However, the same cannot be said for the rear surface, as it seem that the temperature raise with delay, possibly due to inaccurate capturing of the heat transfer within the material.

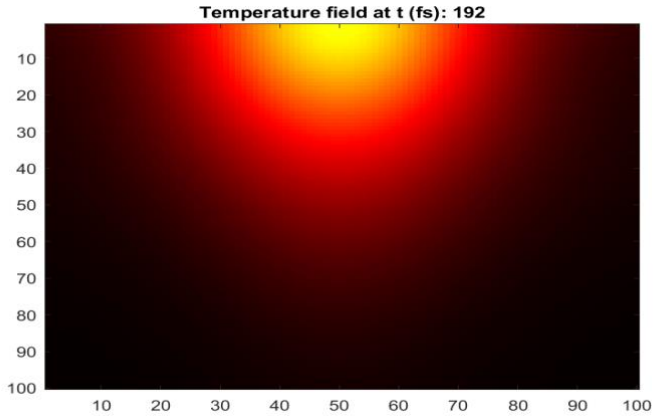

Figure 3: Normalized Electron Temperature profile at $t = 192fs$

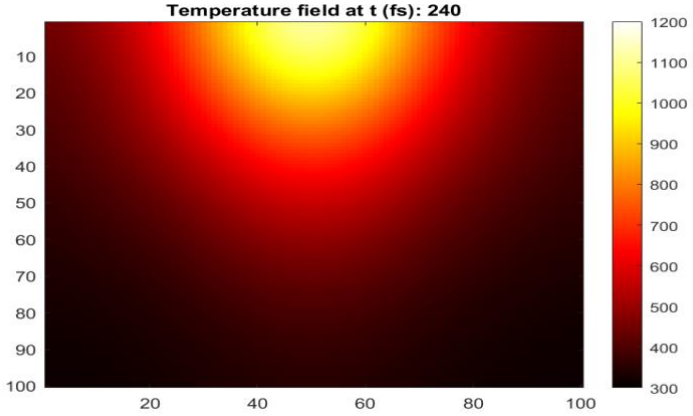

Figure 4: Normalized Electron Temperature profile at $t = 240fs$

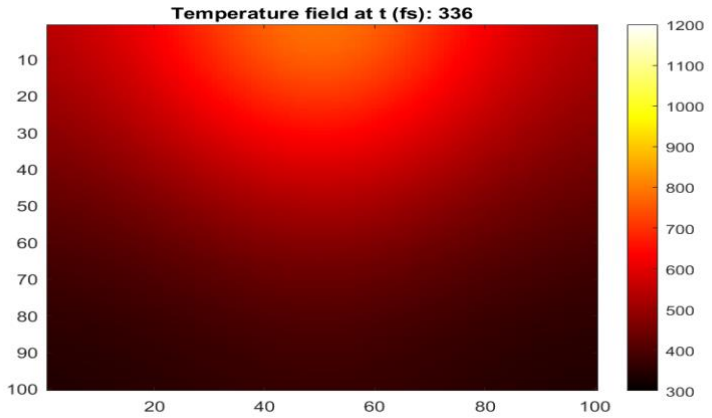

Figure 5: Normalized Electron Temperature profile at $t = 336fs$

The temperature profile at certain times given in figures ?? shows its evolution of how heat is transferred from the laser to electron. Since the boundaries are treated as adiabatic for both electron and lattices, the electron loses its energy only from energy transfer towards the lattice, while the lattices do not lose energy, as shown in Fig. 6.

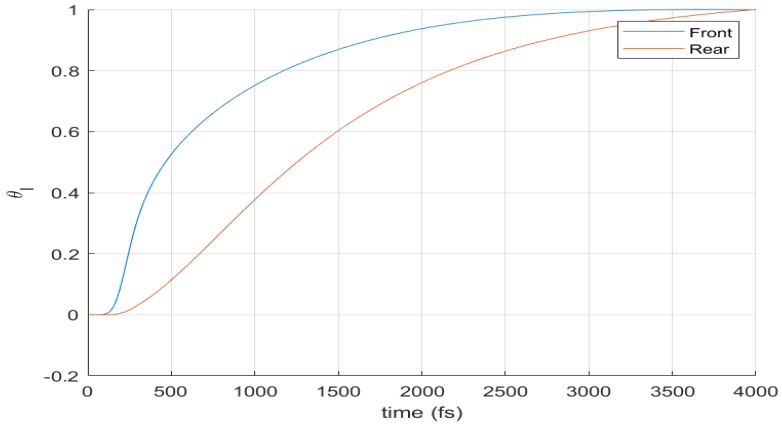

Figure 6: Normalized lattice temperature in the front surface and rear surface of gold for $K = 10J/m^2$, $d = 100nm$

4. CONCLUSION

The numerical framework for hyperbolic lattice Boltzmann is currently on progress. Results has shown promising potential for the use of HLBM in multidimensional LIPSS study. However, some fixes and improvement on numerical code is still needed.

Future Work

The study of ablation threshold by phase explosion can be analysed when the verified results are acceptable. This can be done by disintegrating grids in which the lattice temperature reaches a certain threshold

The Two Temperature Model on its own is still limited for describing other ablation mechanism. In order to model more complex ablation such as capillaries and multipulse dynamics, a modified TTM is required, such as TTM-Maxwell Model and TTM-Phase Field Model. In addition, hydrodynamic equations may be coupled for better understanding of the disintegration residue.

5. REFERENCE

[1] S. Tan, J. Wu, Y. Zhang, M. Wang, and Y. Ou, "A Model of Ultra-Short Pulsed Laser Ablation of Metal with Considering Plasma Shielding and Non-Fourier Effect," *Energies*, vol. 11, no. 11, p. 3163, Nov. 2018.

[2] E. Yakovlev, G. Shandybina, and A. Shamova, "Modelling of the heat accumulation process during short and ultrashort pulsed laser irradiation of bone tissue," *Biomed. Opt. Express*, vol. 10, no. 6, p. 3030, Jun. 2019.

[3] C. Latz, T. Asshauer, C. Rathjen, and A. Mirshahi, "Femtosecond-Laser Assisted Surgery of the Eye:

Overview and Impact of the Low-Energy Concept," *Micromachines*, vol. 12, no. 2, p. 122, Jan. 2021.
[4] L. Jiang, A. D. Wang, B. Li, T. H. Cui, and Y. F. Lu, "Electrons dynamics control by shaping femtosecond laser pulses in micro/nanofabrication: Modeling, method, measurement and application," *Light Sci. Appl.*, vol. 7, no. 2, pp. 1–27, 2018.
[5] L. Jiang and H. L. Tsai, "Prediction of crater shape in femtosecond laser ablation of dielectrics," *J. Phys. D. Appl. Phys.*, vol. 37, no. 10, pp. 1492–1496, May 2004.
[6] S. Song *et al.*, "A critical review on the simulation of ultra-short pulse laser-metal interactions based on a two-temperature model (TTM)," *Opt. Laser Technol.*, vol. 159, p. 109001, Apr. 2023.
[7] A. Rudenko, C. Mauclair, F. Garrelie, R. Stoian, and J.-P. Colombier, "Amplification and regulation of periodic nanostructures in multipulse ultrashort laser-induced surface evolution by electromagnetic-hydrodynamic simulations," *Phys. Rev. B*, vol. 99, no. 23, p. 235412, Jun. 2019.
[8] E. G. Gamaly and A. V. Rode, "Physics of ultra-short laser interaction with matter: From phonon excitation to ultimate transformations," *Prog. Quantum Electron.*, vol. 37, no. 5, pp. 215–323, Sep. 2013.
[9] L. Jiang and H.-L. Tsai, "Improved Two-Temperature Model and Its Application in Ultrashort Laser Heating of Metal Films," *J. Heat Transfer*, vol. 127, no. 10, pp. 1167–1173, Oct. 2005.
[10] P. Ji and Y. Zhang, "Multiscale modeling of femtosecond laser irradiation on a copper film with electron thermal conductivity from ab initio calculation," *Numer. Heat Transf. Part A Appl.*, vol. 71, no. 2, pp. 128–136, Jan. 2017.
[11] T. Q. Qiu and C. L. Tien, "Heat Transfer Mechanisms During Short-Pulse Laser Heating of Metals," *J. Heat Transfer*, vol. 115, no. 4, pp. 835–841, Nov. 1993.
[12] Y. T. Lee and R. M. More, "An electron conductivity model for dense plasmas," *Phys. Fluids*, vol. 27, no. 5, pp. 1273–1286, May 1984.
[13] J. K. Chen, W. P. Latham, and J. E. Beraun, "The role of electron–phonon coupling in ultrafast laser heating," *J. Laser Appl.*, vol. 17, no. 1, pp. 63–68, Feb. 2005.
[14] J. M. Liu, "Simple technique for measurements of pulsed Gaussian-beam spot sizes," *Opt. Lett.*, vol. 7, no. 5, p. 196, May 1982.
[15] M. Ciesielski and B. Mochnacki, "Hyperbolic model of thermal interactions in a system biological tissue—protective clothing subjected to an external heat source," *Numer. Heat Transf. Part A Appl.*, vol. 74, no. 11, pp. 1685–1700, Dec. 2018.
[16] Y. Guo and M. Wang, "Phonon hydrodynamics for nanoscale heat transport at ordinary temperatures," *Phys. Rev. B*, vol. 97, no. 3, p. 035421, Jan. 2018.
[17] Z. M. Zhang, *Nano/Microscale Heat Transfer*. Cham: Springer International Publishing, 2020.
[18] Y. Liu, L. Li, and Q. Lou, "A hyperbolic lattice Boltzmann method for simulating non-Fourier heat conduction," *Int. J. Heat Mass Transf.*, vol. 131, pp. 772–780, Mar. 2019.
[19] J. Zhang, Y. Chen, M. Hu, and X. Chen, "An improved three-dimensional two-temperature model for multi-pulse femtosecond laser ablation of aluminum," *J. Appl. Phys.*, vol. 117, no. 6, Feb. 2015.
[20] S. D. Brorson, J. G. Fujimoto, and E. P. Ippen, "Femtosecond electronic heat-transport dynamics in thin gold films," *Phys. Rev. Lett.*, vol. 59, no. 17, pp. 1962–1965, Oct. 1987.